의학박사 학위논문

Resistance Mechanism to Histone Deacetylase Inhibitor in Non-small Cell Lung Cancer

비소세포폐암에서 히스톤탈아세틸화제에 대한 내성 기전

2014 년 **2** 월

서울대학교 대학원
의학과 분자종양의학 전공
김진수

비소세포폐암에서 히스톤탈아세틸화제에 대한 내성 기전

지도 교수 방 영 주

이 논문을 의학박사 학위논문으로 제출함

2013 년 **11** 월

서울대학교 대학원

의학과 분자종양의학 전공

김 진 수

김진수의 의학박사 학위논문을 인준함

2014 년 **1** 월

위 원 장 _____ **(인)**

부위원장 _____ **(인)**

위 원 _____ **(인)**

위 원 _____ **(인)**

위 원 _____ **(인)**

Resistance Mechanism to Histone Deacetylase Inhibitor in Non-small Cell Lung Cancer

by
Jin Soo Kim
(Directed by Yung-Jue Bang, M.D., Ph.D.)

A thesis submitted to the Department of Medicine in partial fulfillment of the requirements for the Degree of Doctor of Philosophy in Medical Science (Molecular Oncology) at Seoul National University College of Medicine

Jan 2014

Approved by Thesis Committee:

Professor _____ **Chairman**
Professor _____ **Vice chairman**
Professor _____
Professor _____
Professor _____

Resistance Mechanism to Histone Deacetylase Inhibitor in Non-small Cell Lung Cancer

By Jin Soo Kim

Department of Medicine (Molecular Oncology), Seoul National University College of Medicine

Abstract

Background: Histone deacetylase (HDAC), which modulate chromatin structure and gene expression, has attracted attention as a promising therapeutic target for hematologic and solid tumors including non-small cell lung cancer (NSCLC). However, the mechanisms resulting in the resistance to HDAC inhibitors are not yet well-known. In the current study, the involvement of insulin-like growth factor 1 receptor (IGF-1R) signaling was investigated in resistance to HDAC inhibitors in NSCLC.
Material and Methods: Response to vorinostat was tested in a panel of 14 NSCLC cell by MTT assay. Because cells growing in monolayers on standard tissue culture plates (TCPs) could have different response to drug treatment compared with cells growing in vivo, which is three-dimensional (3D), the effects of vorinostat were also tested on the cells

cultured in soft agar. After the identification of sensitive and resistant cells, receptor tyrosine kinase (RTK) array was performed to elucidate the culprit growth factor signaling pathway. Western blot analysis or real time quantitative PCR were done to confirm the biochemical changes. The antitumor effects of vorinostat, either alone or in combination with the culprit pathway inhibitor would be evaluated using representative vorinostat-resistant NSCLC cell lines. The antitumor potency of vorinostat, either single or in combination with culprit pathway inhibitor on the growth of NSCLC was evaluated using xenograft tumors of two NSCLC cell lines grown in nude mice.

Results: Based on MTT assay, IC_{50} values were measured in each cell lines. In relatively resistant cells, vorinostat seemed to induce expression of phosphorylated IGFR (p-IGFR) in dose and time dependent manner. In contrast, expression of p-IGFR in relatively sensitive cells, tended to decrease. Addition of anti-IGF-1R monoclonal antibody dalotuzumab increased cytotoxicity in relatively resistant cells in soft agar colony forming assay. Real-time quantitative PCR revealed significant increases of IGF-2 in the primary and acquired resistant cells. In xenograft model, combined treatment of vorinostat and dalotuzumab significantly delayed tumor growth compared with vehicle only or single agent treatment.

Conclusions: Our results suggested that (a) resistance to vorinostat might be related to activation of IGF-IR and (b) the combination of

dalotuzumab could overcome the resistance to vorinostat *in vitro* and *in vivo*.

Keyword: Non-small cell lung cancer, histone deacetylase inhibitor, insulin-like growth factor, resistance mechanism

Student number: 2005-30674

Contents

List of Tables

List of Figures

I. Introduction

Non-small cell lung cancer (NSCLC) is the leading cause of cancer-related deaths in the United States (1), and current systemic therapies for NSCLC have limited efficacy, indicating the need for novel treatment strategies (2). Current standard treatments for NSCLC, such as platinum or taxanes based combination chemotherapy, have been shown to result in a modest increase in survival and relief of cancer-related symptoms, which seems to have reached a plateau of effectiveness. The addition of bevacizumab (3) or cetuximab (4) increase survival of NSCLC patients in pivotal phase III trials, but the observed benefits were 2 months at most. Erlotinib or gefitinib are very effective in 10-20% of NSCLC patients with EGFR mutation or amplification. A recent study of crizotinib in patients with EML4-ALK translocation showed striking efficacy (5), but the patient who might benefit from the treatment would be 3-5% of all NSCLC patients. The treatment of NSCLC is therefore a major unmet need and new therapies focusing on the molecular mechanisms that mediate the growth of lung cancer are urgently needed.

Epigenetic changes, such as protein acetylation on lysine residues by histone acetyltransferases (HATs) and deacetylation by histone deacetylases (HDACs), may play an important role in the regulation of gene expression through both chromatin remodeling (by

histone acetylation) and acetylation of transcription factors. Histone deacetylase (HDAC) inhibitors are members of a novel class of anticancer agents that act by regulating chromatin structure and function (6). Vorinostat is a hydroxamic acid multi-HDAC inhibitor that blocks the enzymatic activity of both Class I (HDAC1,-2, and -3) and Class II (HDAC6) HDACs at low nanomolar concentrations (IC50 < 86 nM) by directly binding to the catalytic site of these enzymes (7). Phase I studies with pharmacokinetic analysis showed that serum levels in treated patients reached 0.43 to 2.98 μmol/L (8, 9). The mechanism of the anticancer effects of vorinostat are not completely understood, but it has been shown to have multiple protein targets whose acetylation selectively alters the transcription of genes and the function of proteins that are regulators of proliferation, migration and death of transformed cells (10). Vorinostat showed a promising activity of 30% for patients with progressive, persistent, or recurrent cutaneous T-cell lymphoma (CTCL) (11) and subsequently was approved by the US Food and Drug Administration in 2006. This approval was based on a pivotal Phase IIb multicenter trial of vorinostat monotherapy, which included 74 patients with persistent, progressive or recurrent, stage IB or higher CTCL who had received at least two prior systemic therapies (12).

Several studies have showed a promising efficacy of vorinostat for lung cancer. Vorinostat induced a significant G0-G1 growth arrest of NSCLC cells with induction of expression of $p21^{WAF1}$

(13). Recently, clinical trials involving vorinostat in patients with NSCLC were reported. In phase II trial, vorinostat showed disease stabilization as monotherapy in patients with relapsed NSCLC (14). Because vorinostat exhibited synergistic anticancer effects when given in combination with taxanes and platinum compounds in NSCLC cells (15) and encouraging anticancer activity was noted in NSCLC patients in phase I trial for these combinations (8), there was a randomized phase II trial comparing paclitaxel/carboplatin (PC) +/- vorinostat (16). The objective response rate was improved from 12.5% to 34% (P = 0.021), but, there was only a trend toward improvement in median progression-free survival (6.0 months v 4.1 months; P = 0.48) and overall survival (13.0 months v 9.7 months; P = 0.17) in the vorinostat arm, even though this study do not have enough power for survival. Unfortunately, a phase III trial comparing PC versus PC with vorinostat has been recently terminated based on the recommendation by the DSMB following a pre-planned protocol interim analysis because the endpoint was not achieved (http://www.clinicaltrials.gov, NCT00473889).

These data suggests that significant number of patients does not benefit from the addition of vorinostat and responding patients would eventually show clinical resistance to vorinostat. Drug resistance is a common problem associated with chronic treatment with any anticancer drugs. The aim of this study was to elucidate the possible mechanism of vorinostat resistance in NSCLC cells.

II. Methods

1) Cells and reagents

Human non-small cell lung cancer cell lines H226B, H226Br, H292, H322, H358, H427, H460, H596, H1299, H1944, H1993, H2126, A549 and A549M were obtained from the American Tissue Culture Collection. While cells other than H427 were cultured in RPMI 1640, H427 cells were cultured in DMEM/F12, supplemented with 10% fetal bovine serum (FBS) and antibiotics at 37°C in a humidified environment with 5% CO_2. Clinical-grade vorinostat and dalotuzumab were provided by Merck & Co. Stock solutions of vorinostat were prepared as 20 m*M* stock solutions in dimethyl sulfoxide (DMSO), stored at –20 °C and diluted to appropriate concentrations in culture medium before addition to the cells. Dalotuzumab were kept in the original container at 4°C.

2) Establishment of a vorinostat-resistant cell line

To create a vorinostat-resistant cell line, the H1944 cells were exposed to 0.2 μM vorinostat for 48 h in RPMI plus 10% FBS. After exposure to vorinostat, they were washed and cultured in drug-free medium until the surviving population of cells was grown to 80% confluence. The surviving cells were continuously exposed to

increasing dosages and these doses were sequentially increased to 0.5 μM (2 months), 1 μM (2 months), 2 μM (2 months), and finally to a concentration of 5 μM vorinostat. The established resistant cell line (H1944/R) was maintained by culture in a medium containing 5 μM vorinostat. For all the in vitro studies, the resistant cells were cultured in drug-free medium for at least 1 week to eliminate the effects of vorinostat.

3) Fluorescence-activated cell sorting (FACS) assays

Human NSCLC cells were plated at a concentration of 5×10^5 cells on 60-mm plates. The cells were treated with either DMSO 0.1% or vorinostat (5 μM) and incubated in RPMI supplemented with 10% FBS for 3 days. For FACS analysis, all cells (i.e., nonadherent and adherent) were harvested and processed using the Annexin V-FITC kit (Cat# 33-1200, Invitrogen, Camarillo, CA) according to the manufacturer's recommendation. Finally, cells were used for fluorescence-activated cell sorting (FACS) assays to analyze apoptosis. The number of apoptotic cells is represented by the number of FITC-positive cells of the total 10,000 gated cells. The percentage of dead cells was determined using a FACScan flow cytometer (Becton Dickinson, San Jose, CA). Representative results from two independent experiments were presented.

4) Western blot analysis

Whole-cell lysates were prepared in lysis buffer as described elsewhere (17). Complete protease inhibitor cocktail (Roche, Alameda, CA) with 1M NaF, 1M β-glycerophosphate and 0.2M Sodium orthovanadate was added to lysis buffer before use. Protein concentrations were measured using the Bio-Rad protein assay (Bio-Rad Laboratories). Equivalent amounts of protein (25–50 µg) were resolved by SDS–polyacrylamide electrophoresis in 6%–12% gels (80 V for 20 minutes and 100 V for 1 hour) and transferred by electroblotting overnight at 20 V to a nitrocellulose membrane (Bio-Rad Laboratories, Hercules, CA). After nonspecific binding to the blot was blocked in Tris-buffered saline (TBS) containing 0.05% Tween 20 (TBST) and 5% nonfat powdered milk, the blot was incubated with primary antibody at the appropriate dilution in TBS–5% bovine serum albumin at 4° C for 16 hours. The membrane was then washed multiple times with TBST and incubated with the appropriate horseradish peroxidase–conjugated secondary antibody for 1 hour at room temperature. The protein–antibody complexes were detected by using the enhanced chemiluminescence kit (Amersham, Arlington Heights, IL), according to the manufacturer's recommended protocol. Loading and transferring control was confirmed by probing the membranes with anti-ß-actin antibody.

The following antibodies were used for Western blotting. Phospho-IGF-1R antibody (no. 3021), EGFR antibody (no. 2232), CTCF antibody (no. 2889), poly ADP-ribose polymerase (PARP) antibody (no. 9542), mTOR antibody (no. 2983), phospho-mTOR (no. 2971), Akt antibody (no. 9272), phospho-Akt (Ser473) antibody (no. 9271), and phospho- ERK1/2 antibody (no. 9106) were purchased from Cell-Signaling Biotechnology. IGF-1R (no. 713), ERK antibody (no. 93-G) and β-actin (no. 1675) were purchased from Santa Cruz Biotechnology.

5) Quantitative real-time reverse transcription-PCR

Quantitative real-time reverse transcription PCR was performed using SYBR Green with an ABI PRISM 7700 sequence detection system (Applied Biosystems). Relative quantification of gene expression was performed using the comparative cycle threshold method according to the protocol of the manufacturer (user bulletin no. 2, ABI PRISM 7700 Sequence Detection System; Perkin-Elmer). The relative expression of the target genes was calculated as 2-(ΔCT) with the difference (Δ) between the cycle threshold for the target gene and that for the control gene (L32, ribosomal protein). Primers used in the quantitative RT-PCR are listed as follows: L32 Forward 5' CAACATTGGTTATGGAAGCAACA, Reverse 5' TGACGTTGTGGACCAGGAACT, IGF1 Forward 5'

ATGTATTGCGCACCCCTCAA, Reverse 5' GGGCACGGACAGAGCG, IGF2 Forward 5' GCGGCTTCTACTTCAGCAG, Reverse 5' CAGGTGTCATATTGGAACAAC and CTCF Forward 5' GAACCCATTCAGGGGAAAAGC, Reverse 5' TCGCAAGTGGACACCCAAATC

6) Cell proliferation assay

Cells were seeded into 96-well microculture plates at 2500 to 10,000 cells per well and allowed to attach for 24 hours. Cells were treated with vehicle (DMSO 0.1%) or indicated concentration of vorinostat or dalotuzumab in the standard culture media for 72 hours. Cell proliferation was measured with the 3-(4,5-dimethylthiazol-2-yl)-2,5-diphenyltetrazolium bromide (MTT) assay. The drug concentrations required to inhibit cell growth by 50% were determined by interpolation from the dose-response curves.

7) Anchorage-independent clonogenic growth assay

For the anchorage-independent clonogenic growth assay, 2.5 to 7.5 x 10^3 cells were suspended in 0.5 mL of 0.4% soft agar that was layered on top of 1 mL of 1% solidified agar in each well of 12-well plates. The plates were then incubated for 10 to 15 days in complete medium containing 0.5, 1 and 5 μmol/L concentrations of vorinostat,

10μg/mL of dalotuzumab, or combination. The medium was changed twice a week during this period, at the end of which tumor cell colonies measuring at least 80 μm were stained in 0.001% crystal violet and counted using ImageJ software (Rasband, W.S., ImageJ, U. S. National Institutes of Health, Bethesda, Maryland, USA, http://rsb.info.nih.gov/ij/, 1997-2009). Mean growth inhibition was calculated by dividing the colony number of each treatment group by the colony number of control group. Expected MGI is calculated by multiplying MGIs by single treatment. Index was calculated by dividing the expected colony number by the observed colony number. An index of > 1 indicates synergistic effect and an index of < 1 indicates less than additive effect.

8) Receptor tyrosine kinase activation profiling

The expression and activation of RTKs and their downstream signaling pathways were analyzed using the Proteome Profiler Array kits (R&D Systems). Cell lysates (500 μg) were incubated with the membrane overnight in the buffer provided according to the manufacturer's protocol. The images were captured and the level of RTK activation was densitometrically quantified with ImageJ software (Rasband, W.S., ImageJ, U. S. National Institutes of Health, Bethesda, Maryland, USA, http://rsb.info.nih.gov/ij/, 1997-2009). The intensity values of the probes and the local background of the probes were log

2 transformed to obtain a more symmetrical distribution, and the difference between these two resulted in a fold change.

9) *In Vivo* Tumor Xenograft Model

After irradiation with 350 rad from a cesium-137 source, xenograft tumors were generated by subcutaneous injection of the H1299, H1944 and H1944/VR cells into the flanks of athymic nude mice (Charles River Laboratories) as described elsewhere (18). Briefly, nude mice were injected at a single dorsal flank site with 1.0×10^7 cells in 100 µL of phosphate-buffered saline (PBS). Injection of these cells into nude mice induced exponentially growing tumors. When tumors reached a volume of 50–75mm^3 (termed day 0 for our experiments), mice were treated with intraperitoneal (IP) injection of vehicle (50% polyethylenglycol 400 in distilled water), vorinostat at 50 mg/kg , dalotuzumab 15mg/kg, or combination twice a day for 15–28 days. Tumor growth was quantified by measuring the tumors in two dimensions with calipers twice a week. Volumes were calculated by the formula $0.5 \times a \times b^2$, where *a* and *b* are the longer and shorter diameters, respectively. Tumor volumes were expressed as the mean and standard error. Mice with necrotic tumors or with tumors that had a diameter of more than 1.5 cm were humanely killed by exposure to CO_2. All animal procedures were performed in accordance with a

protocol approved by the M.D. Anderson Cancer Center Institutional Animal Care and Usage Committee.

10) Statistical Analysis

Data are expressed as the mean and 95% confidence interval from at least triplicate samples. Data were calculated either with the Microsoft Excel software program (version 2007; Microsoft Corporation, Redmond, WA) or in the SPSS statistical program (SPSS version 17; SPSS, Chicago, IL). The statistical significance of differences between groups was analyzed with Mann-Whitney test. All statistical tests were two-sided. A P value of less than 0.05 was considered to be statistically significant.

III. Results

1) Characterization of vorinostat responses in human NSCLC cell lines

Cell proliferation assays were performed in the 14 NSCLC cell lines treated with vorinostat. Treatment with vorinostat at doses ranging from 0.5 to 50 μM exhibited a range of sensitivities after 3-day treatment (Fig. 1). IC_{50} values were not correlated with a specific mutational status or histological subtypes, which is consistent with the previous observation with trichostatin A or vorinostat on NSCLC cells (19). To see if the resistance recapitulates in anchorage independent condition, soft agar colony forming assay was done. When the relative number of colonies were calculated by dividing the colony number of control (DMSO 0.1%) and arranged by the decreasing order, the 5 resistant cells were again clustered in the resistant group (Fig 2).

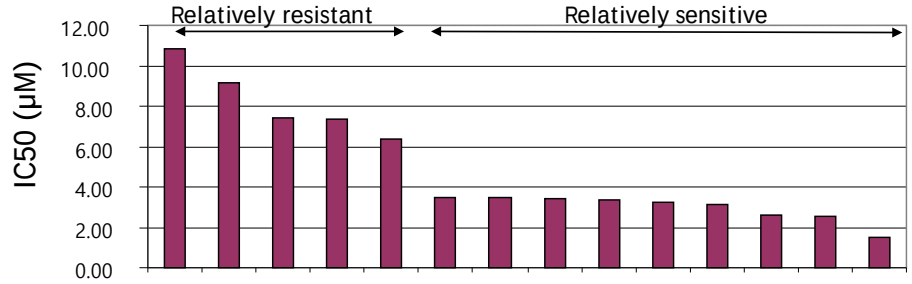

	226Br	596	460	226B	1299	322	2126	292	358	1944	1993	549M	427	549
EGFR	W	W	W	W	W	W	W	W	W	W	W	W	W	W
K-ras	M	W	M	W	W	W	W	W	M	M	W		M	M
P53	M	M	W	W	N	M	M	W	N	W	M		W	W
PI3K		M	M	W	W	W	W	W	W	U	W		W	W
LKB1		W	M	W	W	U	M	W	W	W	M		M	M
B-raf		W	W	W	W	W	W	W	W	U	W		W	W
Histology	S	AS	L	S	L	A	A	AS	B	A	A	A		A

W: wt. M: mutant, N:null, U: unknown
S: squamous, AS: adenosquamous,. L: large cell, A: adenocarcinoma, B: Bronchioloalveolar carcinoma

Figure 1. IC_{50} values by MTT assays in NSCLC cell lines with various genetic background.

Mutational status or histology information was retrieved from the COSMIC database (http://www.sanger.ac.uk/genetics/CGP/cosmic/).

Five cell lines were allocated as relatively resistant based on this result.

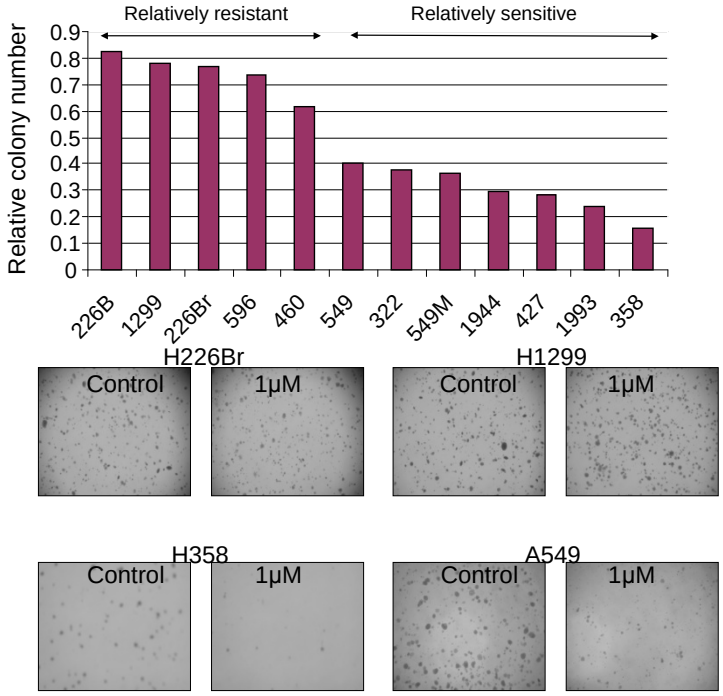

Figure 2. Soft Agar Colony Forming Assay: Relative Colony numbers in Vorinostat 1uM

Relative colony numbers were calculated as the ratio of treated to DMSO treated cells at each dose for each replicate. Representative picture of the colony formation was shown at the bottom.

After the NSCLC cells were treated with dimethyl sulfoxide (DMSO) or the indicated concentration of vorinostat for 72 hr, whole-cell lysates from cells were subjected to immunoblot analysis with the indicated antibodies. Vorinostat induced cleavage of PARP dose-dependently in the representative sensitive cell lines (H1944, Fig 3). Also 5uM of vorinostat could induce apoptosis in sensitive cells (A549, A549M, and H358), while there was no cleavage of PARP in resistance cells (H226Br, H460, H596 and H1299, Fig 4). As shown in Figure 3 and 4, the histone 3 is acetylated in both resistant and sensitive cells, which shows HDAC is inhibited regardless of sensitivity to vorinostat. To confirm the induction of apoptosis, FACS analysis using Annexin-V were performed. Fig.5 showed the induction of apoptosis in the representative sensitive cells (H358 and A549M), while there were no significant increase of Annexin-V positive cell population in the representative resistant cells (H226Br and H1299).

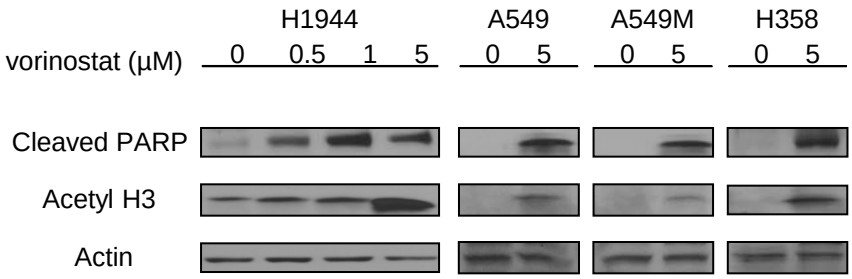

Figure 3. Induction of apoptosis and acetylation of Histone 3 in vorinostat sensitive NSCLC cells

In relatively sensitive NSCLC cells, vorinostat induced apoptosis and acetylation of Histone 3 in dose-dependent manner (H1944). Other sensitive cells (A549, A549M and H358) showed similar response to vorinostat.

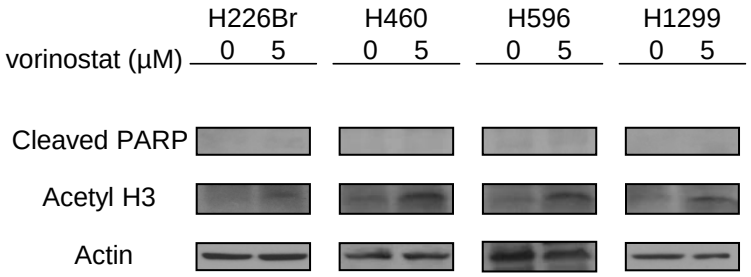

Figure 4. Induction of apoptosis and acetylation of Histone 3 in vorinostat resistant NSCLC cells

In relatively resistant cells, vorinostat induced acetylation of Histone 3, but there was no cleavage of PARP, which means no definitive induction of apoptosis in these cells.

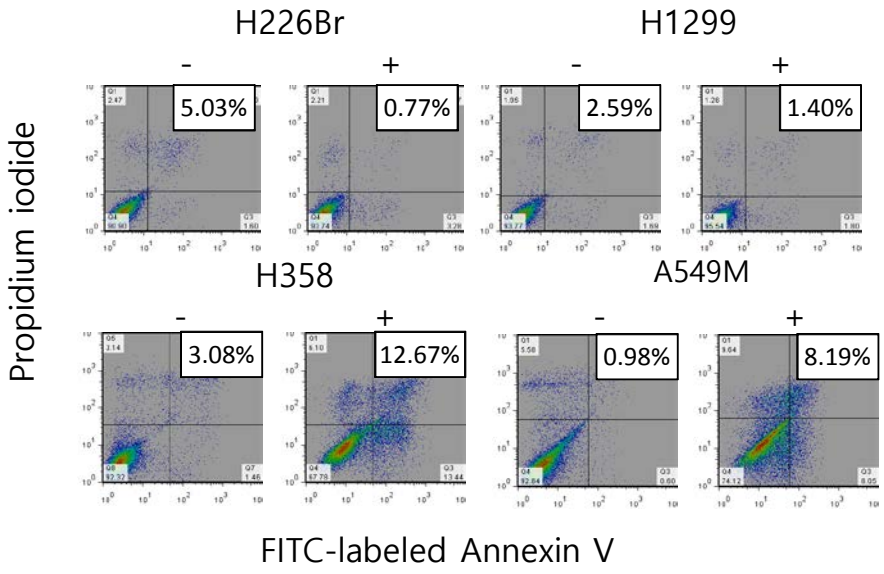

Figure 5. FACS analysis of Annexin V staining in representative resistant and sensitive cells

Cells were treated with 5uM of vorinostat for 48 hours. And the cells were treated with the reagents in the kit, followed by flow cytometric analysis.

2) Representative resistant cells showed an activation of IGF-1R/IR pathway after being treated with vorinostat

To investigate the mechanism of primary resistance to vorinostat, the activation of several tyrosine kinase receptors (RTKs) was examined. Firstly, analysis of RTK phosphorylation using an antibody array suggested that some RTKs were differentially phosphorylated in H1299 cells after vorinostat treatment (Fig 6). The RTK array revealed increased phosphorylations of several receptors after treatment of vorinostat. Data from the average signals (pixel densities) on each array suggested the insulin receptor phosphorylation increased the most after vorinostat treatment among the receptors included in the array (Fig. 7 and 8).

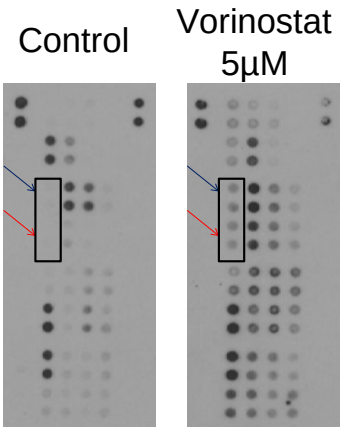

Figure 6. RTK array showed increased phosphorylation of IGF-1R and IR in H1299 cells

Human phospho-RTK array of H1299 cell showed an activation of IGF-1R/IR pathway. H1299 cells were treated with 5μM vorinostat or DMSO for 72 hr in serum deprived condition. Whole-cell lysates were incubated on RTK antibody arrays. Each RTK antibody is spotted in duplicate. Red arrow: insulin receptor, blue arrow: IGF-1R.

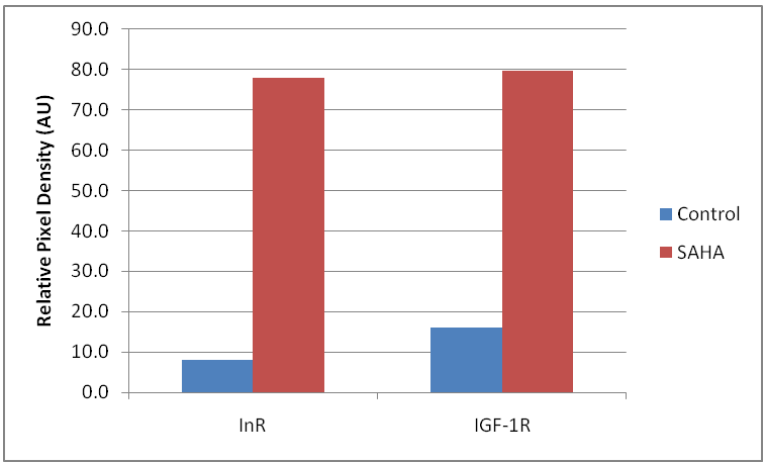

Figure 7. Pixel Quantification of the RTK array

Relative spot densities of each blot and their ratio were shown in the graph. Pixel densities are expressed as percent of the density of control after subtraction of an averaged background signal from each RTK spot.

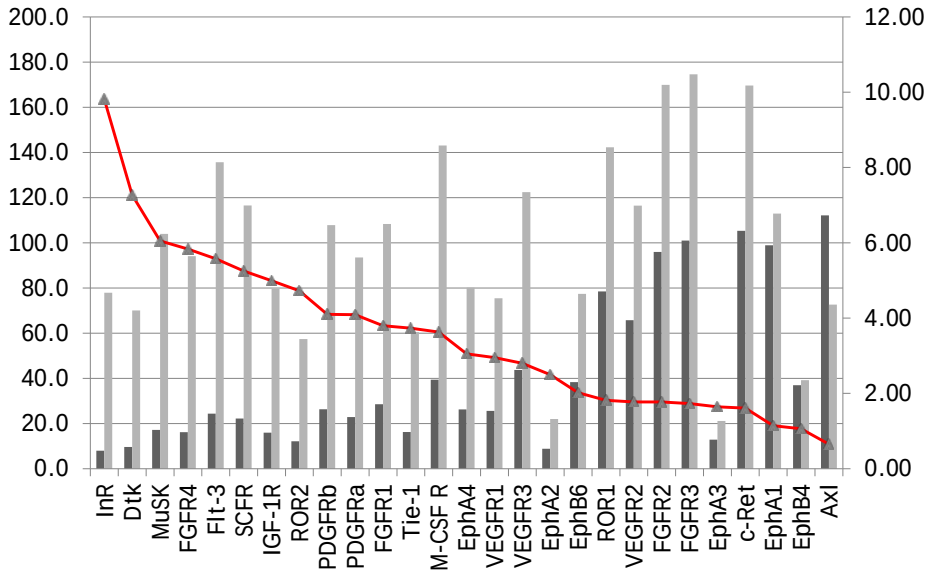

Figure 8. Vorinostat induces RTK activation in H1299 cells

Relative spot densities of each blot (left vertical axis) and their ratio (right vertical axis) were shown in the graph. RTKs are arranged from the highest ratio to the lowest. Pixel densities are expressed as percent of the density of control after subtraction of an averaged background signal from each RTK spot.

Of note, IGF-1R phosphorylation was also increased by the treatment. To validate this observation, Western blotting were performed to test whether the phosphorylation of IGF-1R/IR at Tyr1131, which is indicative of kinase activation, after vorinostat treatment was detectable in the resistant cells. As shown in Fig 9, the phosphorylation of IGF-1R/IR and Akt increases in the representative resistant cells (H226B, H226Br, and H1299), while the phosphorylation decreases or is not shown in the representative sensitive cells (H358, A549, and A549M) in dose dependent manner. In the representative cells, the phosphorylation of IGF-1R/IR and Akt also increases in time-dependent manner (Fig 10).

Taken together, activation of IGF-1R/IR signaling might be correlated with the primary resistance to vorinostat in NSCLC cells.

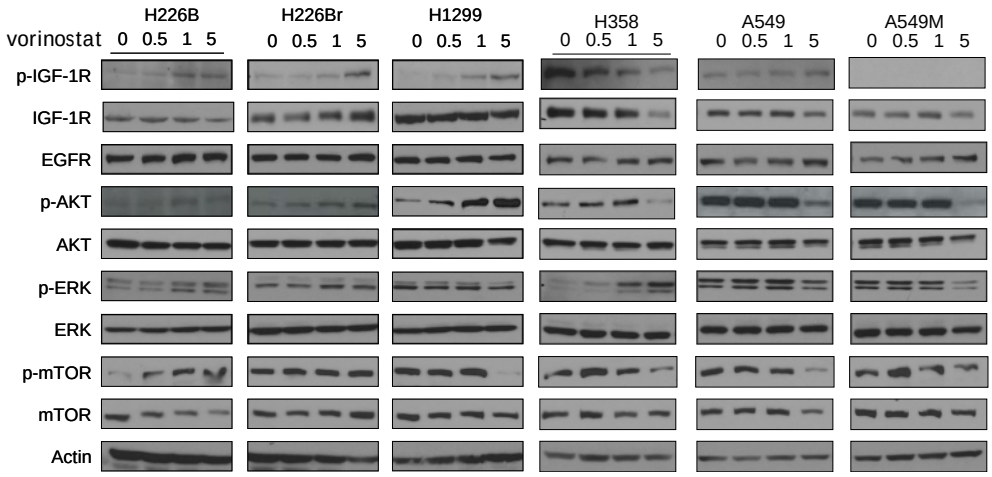

Figure 9. Western blot analysis shows activation of IGF-1R in the resistant cells by vorinostat in dose-dependent manner

Representative resistant cells (H226B, H226Br and H1299) and sensitive cells (H358, A549 and A549M) were treated with the increasing doses of vorinostat (0, 0.5, 1 and 5uM) for 72 hours and subjected to the Western blot analysis. Indicated antibodies were used to reveal the protein expression in the cell lysates.

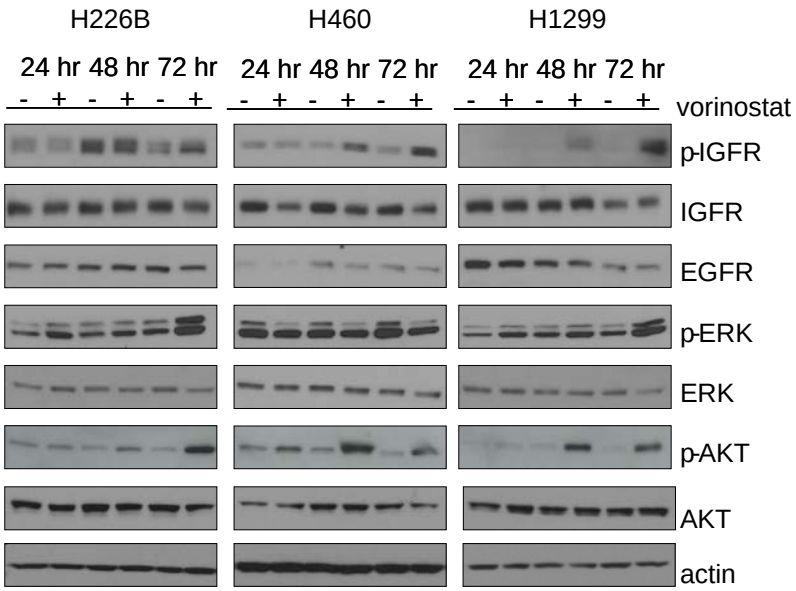

Figure 10. Western blot analysis showed activation of IGF-1R in the resistant cells by vorinostat in time-dependent manner

Representative resistant cells (H226B, H460 and H1299) were treated with vorinostat 5uM or DMSO for 24, 48 and 72 hours and subjected to the Western blot analysis. Indicated antibodies were used to reveal the protein expression in the cell lysates.

3) Effects of dalotuzumab on the relatively resistant cells and synergy with vorinostat

IGF-1R pathway has gained increasing attention as a promising target in cancer treatment, although the efficacy of the inhibition need to be investigated more (20). IGF-1R activation triggers a cascade of reactions involving two signal transduction pathways: one activates Ras, Raf and MAPK, and the other involves PI3K. To investigate if the inhibition of IGF-1R/IR pathway would circumvent the resistance to vorinostat, we analyzed the effect of IGF-1R monoclonal antibody, dalotuzumab on the NSCLC cells. Even though dalotuzumab effectively downregulates IGF-1R expression at a very low dose (Fig 11) in the resistant cells, these IGF-1R inhibitions did not translate into cell growth inhibition, when the response to dalotuzumab upto 100ug/mL was assessed by MTT assay (Fig 12).

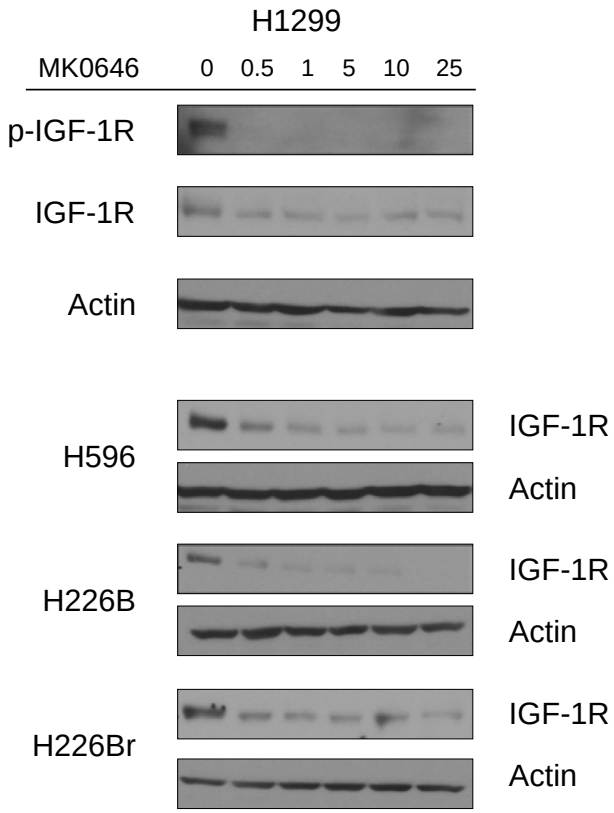

Figure 11. anti-IGF-1R antibody dalotuzumab (MK0646) induces IGF-1R downregulation in vorinostat-resistant cells

With dalotuzumab at low concentrations, IGF-1R expression and p-IGF-1R were effectively downregulated in the vorinostat-resistant cells.

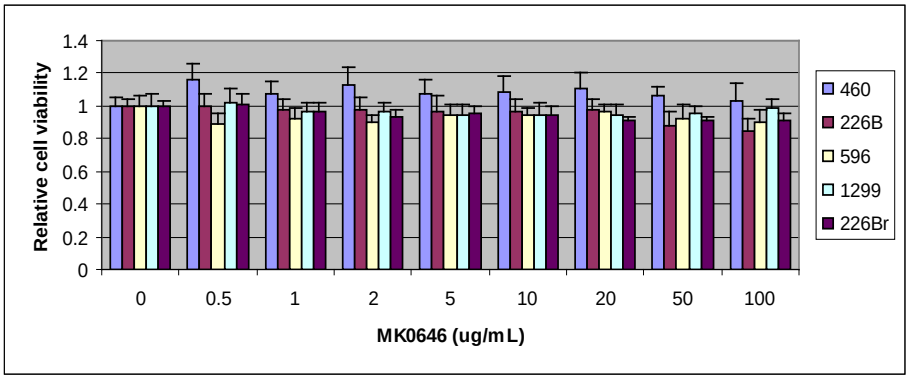

Figure 12. Minimal cytotocixity of dalotuzumab (MK0646) on monolayer culture (MTT assay)

By MTT assays on tissue culture plates, no inhibition of cell proliferation was shown in the vorinostat-resistant cells with dalotuzumab (concentration range: 0 – 100ug/mL)

Because cells growing in monolayer on standard tissue culture plates could have different response to drug treatment compared with cells growing in vivo in three-dimensional (3D) environment, the effects of vorinostat and dalotuzumab was tested on the cells cultured in soft agar, which is 3D-tumor-like microenvironment. As a single treatment, each drug showed some level of growth inhibition in the relatively resistant cells. When combined with dalotuzumab, the growth inhibition was more prominent compared to vorinostat single treatment (Fig 13 and Table 1).

Together, these data suggest that persistent IGF-1R signaling leads to the resistant to vorinostat and the inhibition of IGF-1R pathway by dalotuzumab could effectively reduce cell viability in these vorinostat resistant cells.

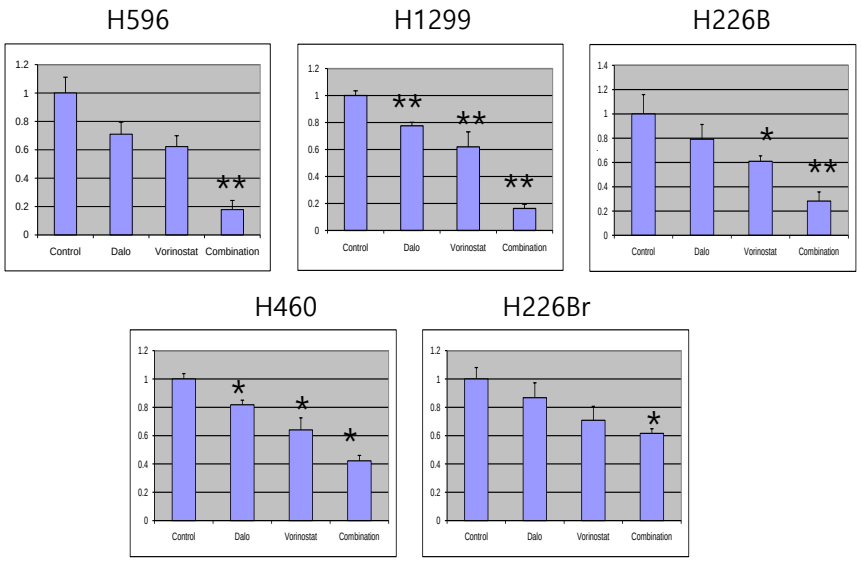

Figure 13. Soft Agar Colony Forming Assay in vorinostat-resistant cells treated with vorinostat with or without dalotuzumab

Relative colony numbers to DMSO treated controls are shown. P-values were calculated by Mann-Whitney test compared to control group * $p < .05$, ** $p < .01$.

Table 1. Combination effect on soft agar colony forming assays

Cell lines	Vorinostat (1uM)		Dalotuzumab (10ug/ml)		Combination			Index[§]
	MGI[*]	P[†]	MGI	P[†]	Expected	Observed	P[‡]	
H460	0.641	.016	0.818	.032	0.524	0.422	.016	1.244
H226B	0.609	.032	0.791	.341	0.482	0.283	.004	1.706
H596	0.623	.095	0.710	.056	0.442	0.178	.004	2.484
H1299	0.669	.008	0.770	.008	0.515	0.175	.008	2.944
H226Br	0.920	0.468	0.781	.114	0.719	0.392	.021	1.83

*MGI (Mean Growth Inhibition) = colony number of treated group/colony number of untreated group. †P-values were calculated by Mann-Whitney test compared to control group. ‡P-value was calculated by Mann-Whitney test compared to SAHA treated group. § Calculated by dividing the expected colony number by the observed colony number. An index of > 1 indicates synergistic effect and an index of < 1 indicates less than additive effect.

4) Chronic exposure to vorinostat leads to acquired drug resistance

To investigate if chronic exposure to vorinostat could lead to acquired drug resistance, vorinostat sensitive H1944 cells were chronically treated with increasing concentrations of vorinostat. MTT assays and soft agar colony forming assay showed that H1944 cells that had been chronically treated with vorinostat (H1944R) required higher doses of the drug for growth inhibition (Fig 14 and 15). The resistant cells are indicated by the name of the parental cell line followed by ‘‘R’’.

Interestingly, we detected increased phosphorylation of IGF-1R and IR in the H1944R cells by vorinostat treatment using human phospho RTK array (Fig 16, 17, 18 and 19), which were also activated in the primary resistant cells (Fig 6 and 7).

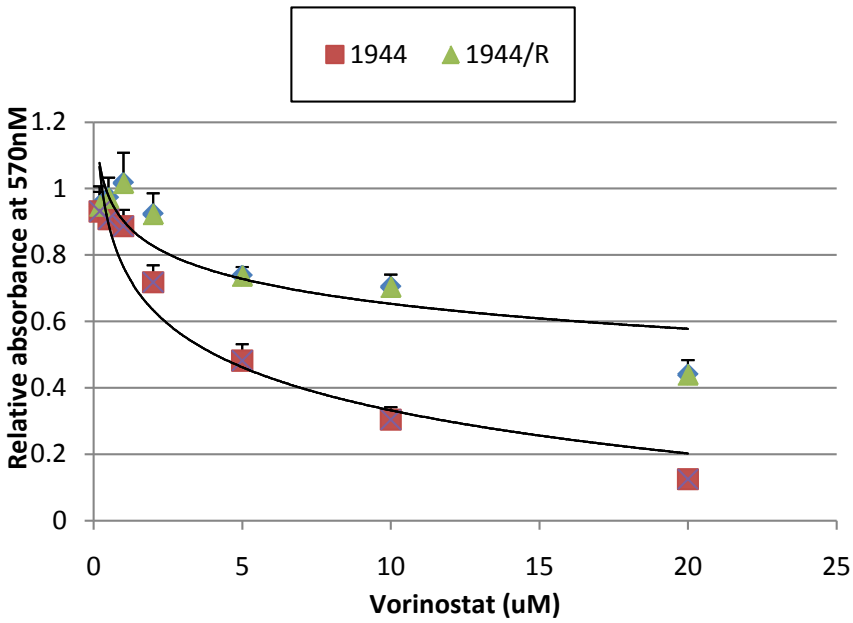

Figure 14. Acquired resistance was induced in H1944 cells (MTT assay)

By MTT assay, H1944/R cells showed higher IC50 compared with the parental H1944 cells at 72 hours of vorinostat treatment.

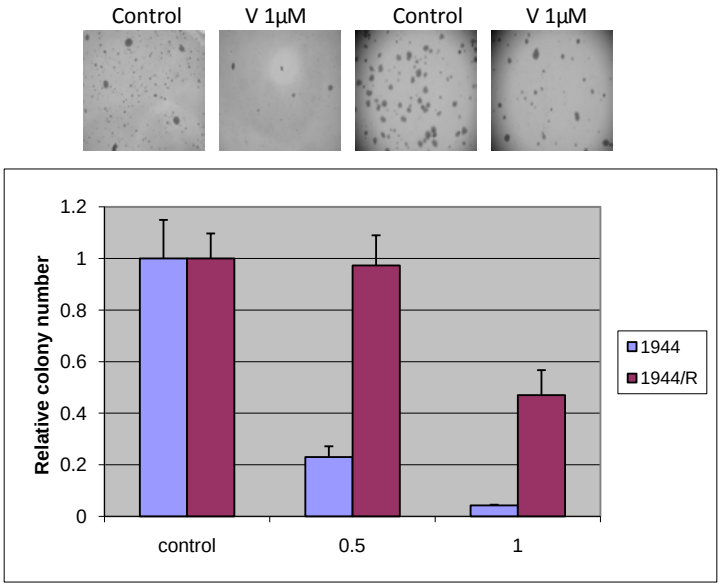

Figure 15. Acquired resistance was induced in H1944 cells (Soft agar colony forming assay)

Representative pictures of colonies were shown at the top, and the relative colony numbers were drawn at the bottom.

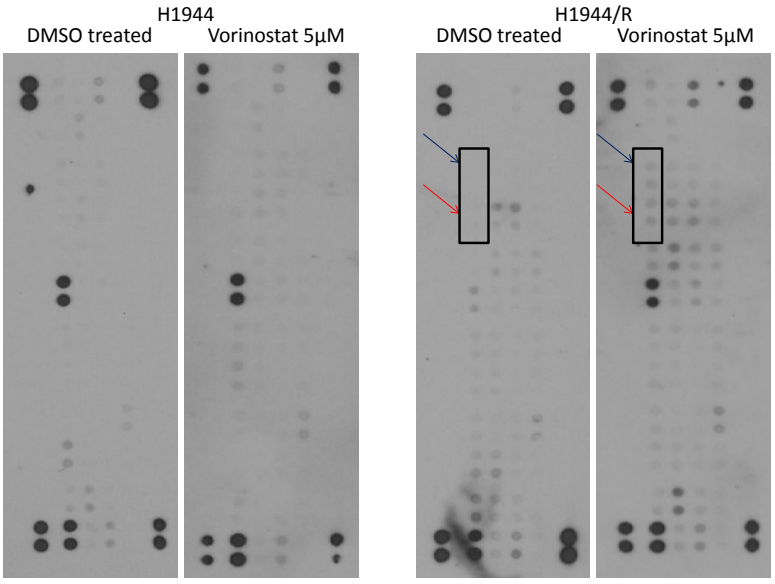

Figure 16. RTK array showed increased phosphorylation of IGF-1R and IR in H1944/R cells

Human phospho-RTK array of H1944 and H1944/R cell showed an activation of IGF-1R/IR pathway in H1944/R cells. Cells were treated with 5μM vorinostat or DMSO for 72 hr in serum deprived condition. Whole-cell lysates were incubated on RTK antibody arrays. Each RTK antibody is spotted in duplicate. Red arrow: insulin receptor, blue arrow: IGF-1R.

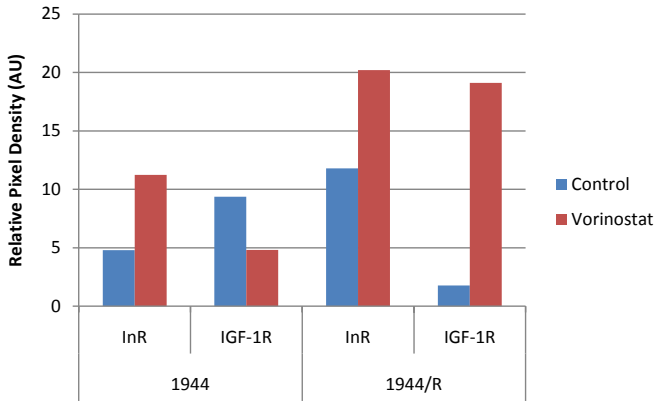

Figure 17. Pixel Quantification of the RTK array

Relative spot densities of each blot and their ratio were shown in the graph. Pixel densities are expressed as percent of the density of control after subtraction of an averaged background signal from each RTK spot.

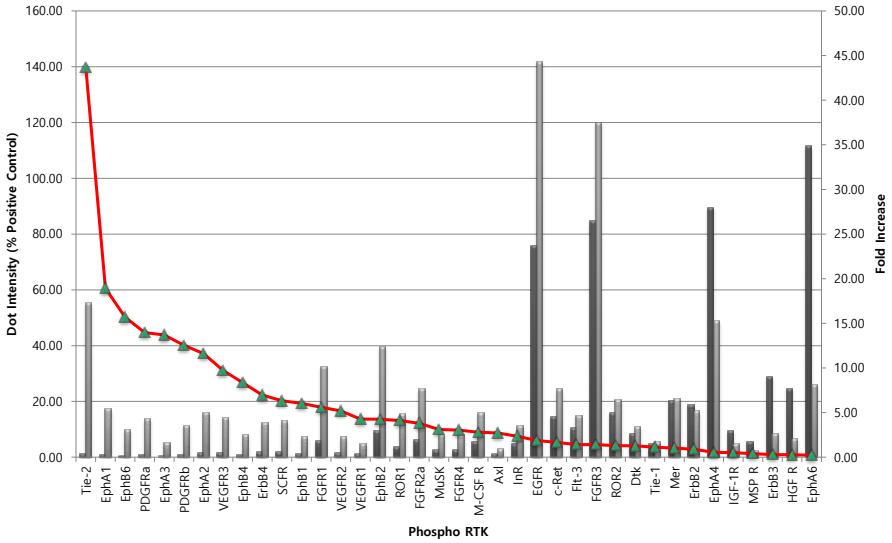

Figure 18. Vorinostat induces RTK activation in H1944 cells

Relative spot densities of each blot (left vertical axis) and their ratio (right vertical axis) were shown in the graph. RTKs are arranged from the highest ratio to the lowest. Pixel densities are expressed as percent of the density of control after subtraction of an averaged background signal from each RTK spot.

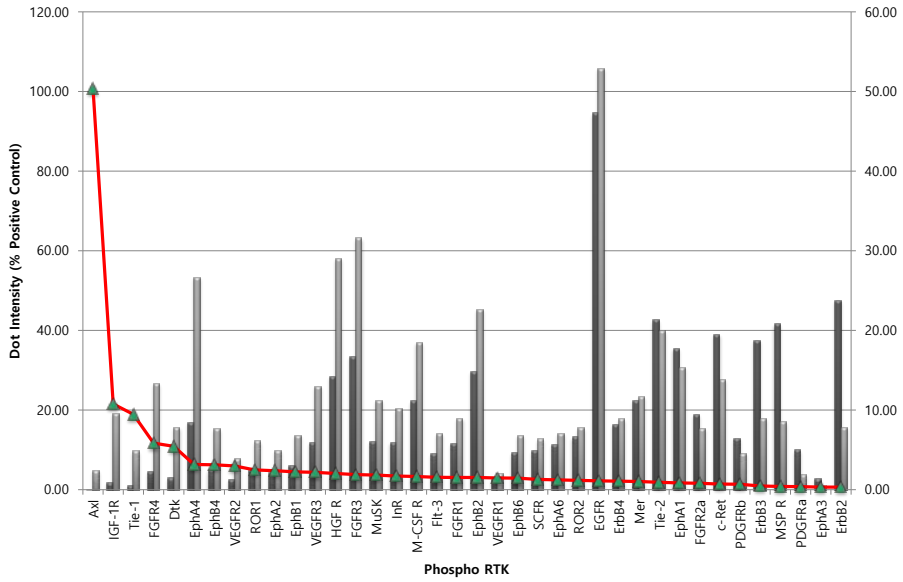

Figure 19. Vorinostat induces RTK activation in H1944/R cells

Relative spot densities of each blot (left vertical axis) and their ratio (right vertical axis) were shown in the graph. RTKs are arranged from the highest ratio to the lowest. Pixel densities are expressed as percent of the density of control after subtraction of an averaged background signal from each RTK spot.

Western blotting confirmed that the resistant cell showed phosphorylation of IGF-1R by vorinostat in dose-dependent manner, while the phosphorylated IGF-1R decreased in parental cells (Fig 20). Also, the addition of dalotuzumab to vorinostat inhibited the colony formation in the H1944/R cells (Fig 21), as shown in the primary resistant cells.

These data demonstrate that chronic treatment with vorinostat can lead to development of drug resistance in NSCLC cells that were initially sensitive, and the cells with acquired resistance. And the activation of IGF-1R pathway might be one of the culprit mechanisms of the resistance. Also, the inhibition of IGF-1R pathway with monoclonal antibody could be an effective way to overcome the resistance.

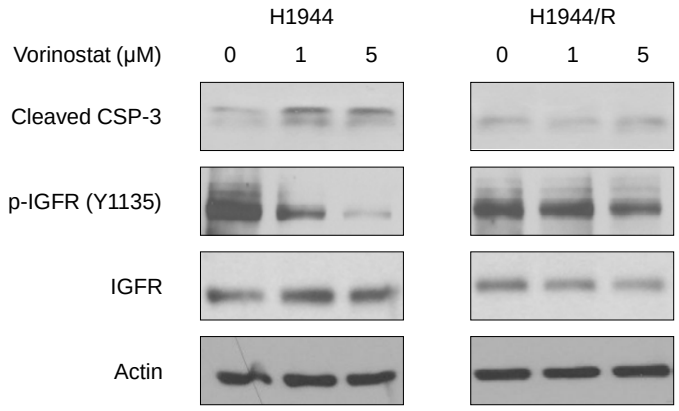

Figure 20. Western blot analysis shows acquired resistance of H1944/R cells to vorinostat

After vorinostat treatment ranging from 0, 1 and 5 μM, caspase-3 was highly activated in H1944 cells compared to H1944/R cells. IGF-1R phosphorylation significantly decreased in H1944 cells while it did not seem to be affected in H1944/R cells.

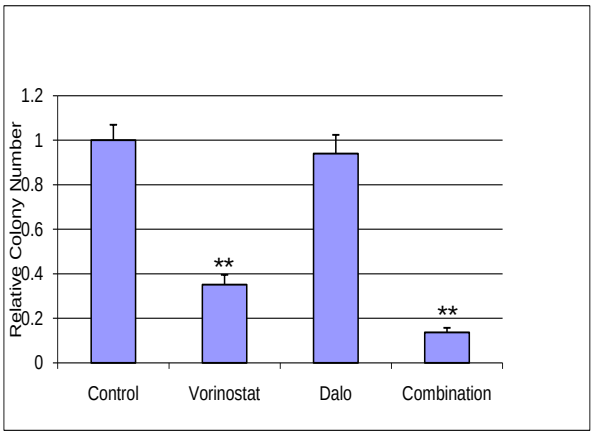

Figure 21. Soft agar colony forming assay shows the combination effect of vorinostat and dalotuzumab in H1944/R cells

Relative colony numbers to DMSO treated controls are shown. Combination treatment with vorinostat (2.5uM) and dalotuzumab (10ug/dL) significantly inhibited the colony formation in H1944/R cells. P-values were calculated by Mann-Whitney test compared to control group, ** $p < .01$.

5) *In vivo* antitumor activity of vorinostat with dalotuzumab against NSCLC xenografts

To assess the efficacy of the vorinostat/dalotuzumab combination in a separate *in vivo* model, nude mice bearing xenografts of H1299 (Fig 22) and H226Br cells (Fig 23) were treated with vorinostat with or without dalotuzumab. In this model, combined treatment of vorinostat and dalotuzumab significantly delayed the growth of H1299 and H226Br xenograft tumors compared to vehicle or single agent treatment.

To investigate whether the combination could also inhibit the tumor growth in cells with acquired resistance, H1944 and H1944R cells were xenografted in nude mice. The mice were treated with vorinostat or vehicle in H1944 model, while those were treated with vehicle, vorinostat, dalotuzumab or the combination in H1944/R model. The growth of xenograft tumor with H1944 cells was delayed by vorinostat treatment, while that with H1944R cells was not inhibited by vorinostat treatment (Fig 24 and Fig 25). Consistent with xenograft model in the primary resistance cells, the combination of dalotuzumab and vorinostat was able to delay tumor growth compared to either agent alone (Fig 25).

The collective data suggest that targeting IGF-1R with dalotuzumab can result in antitumor activity in NSCLC cells primarily

resistant to vorinostat as well as cells with acquired resistance to vorinostat *in vitro* and *in vivo*.

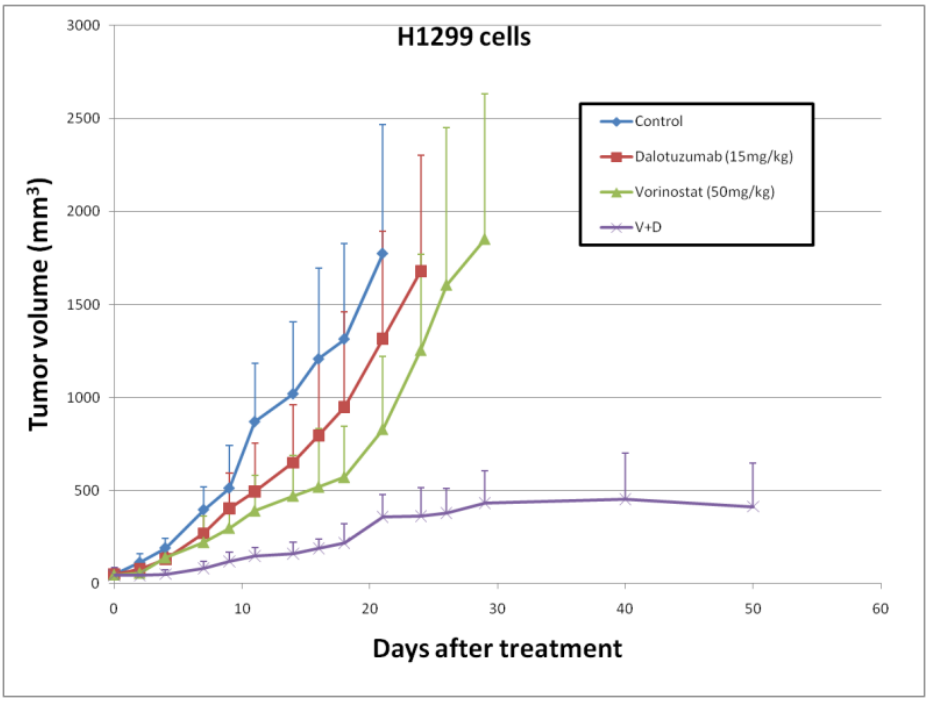

Figure 22. Tumor xenograft model with H1299 cells in nude mice

Each treatment group had either 7 or 8 mice. Vorinostat 50mg/kg, dalotuzumab 15mg/kg or the combination were given i.p. twice a week. D=dalutuzumab, V=vorinostat

Control vs V+D, p <.05 (from D11), V or D vs. V+D, p=not significant

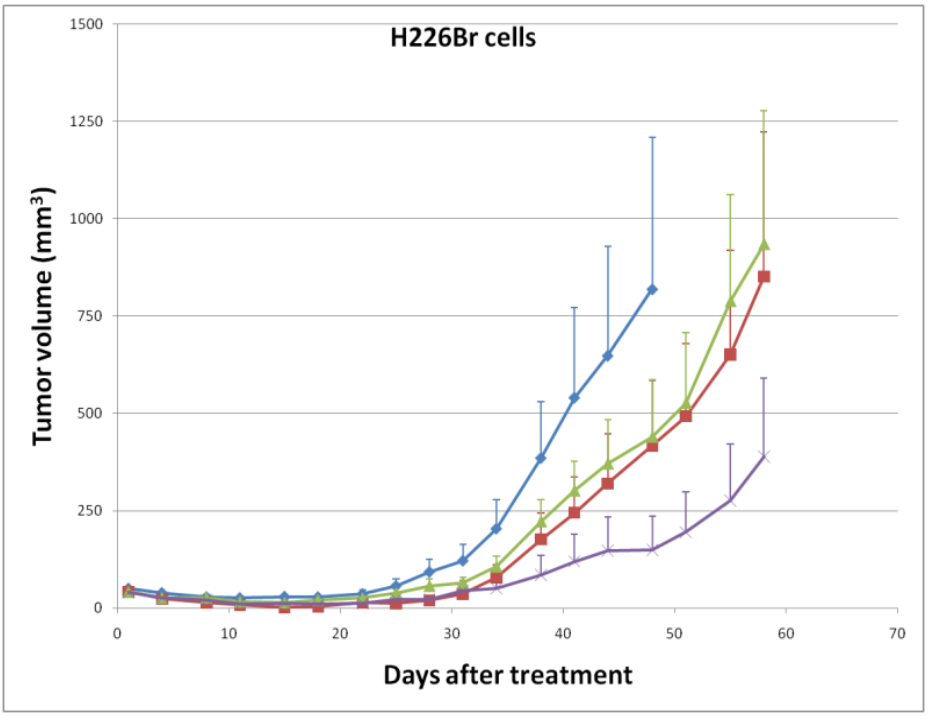

Figure 23. Tumor xenograft model with H226Br cells in nude mice

Each treatment group had either 7 or 8 mice. Vorinostat 50mg/kg, dalotuzumab 15mg/kg or the combination were given i.p. twice a week.

D=dalutuzumab, V=vorinostat

Control vs V+D, p <.05 (from D38)

V or D vs. V+D, p=not significant

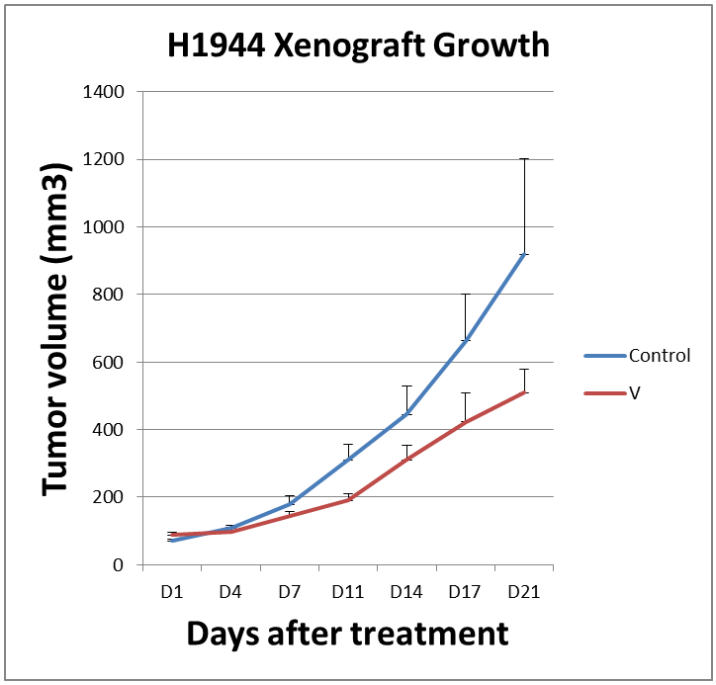

Figure 24. Tumor xenograft model with H1944 cells in nude mice

Each treatment group had either 7 or 8 mice. Vorinostat 50mg/kg was given i.p. twice a week.

V=vorinostat

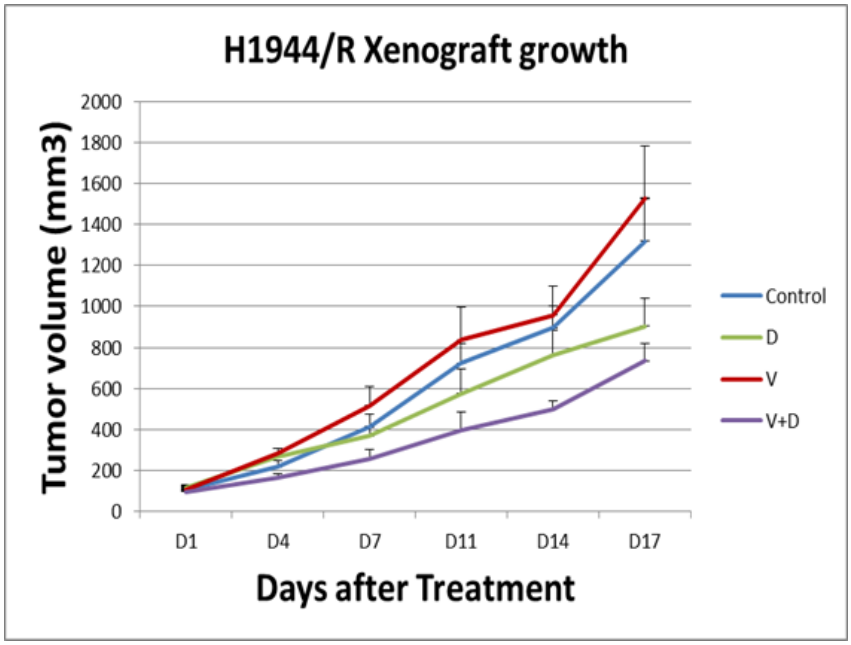

Figure 25. Tumor xenograft model with H1944/R cells in nude mice

Each treatment group had either 7 or 8 mice. Vorinostat 50mg/kg, dalotuzumab 15mg/kg or the combination were given i.p. twice a week. D=dalutuzumab, V=vorinostat

6) Increased IGF-2 transcription in the resistant cells

The present study showed increased phosphorylation of IGF-1R/IR without significant change of IGF-1R expression, which suggests receptor activation by the ligands. To evaluate the potential mechanism of IGF-1R/IR activation, we examined the changes of IGF-1 and IGF-2 transcription after vorinostat exposure with quantitative real-time reverse transcription-PCR. While IGF-1 transcription was not greatly affected by vorinostat in both resistant and sensitive cells (Fig 26), IGF-2 transcription was greatly induced by vorinostat in resistant cells (Fig 27). In H1944R cells, IGF-2 transcription was also greatly increased by vorinostat, while that was slightly increased in the parental cells (Fig 28) and IGF-1 transcription was not significantly affected in both cells (Fig 29).

These data suggest the activation of IGF-1R in the primary and acquired resistant cells might be influenced by the increased IGF-2 transcription, not by the changes IGF-1 mRNA levels.

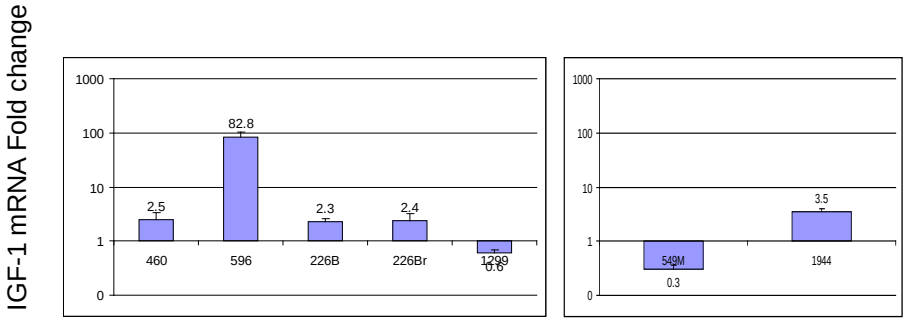

Figure 26. IGF-1 mRNA fold changes in the resistant and sensitive cells

RNA was isolated 48 h after 5uM of vorinostat treatment, and mRNA levels of IGF-1 and L32 were determined by quantitative real-time PCR. After the normalization by L32 control, mRNA expression levels between the untreated and vorinostat-treated samples in the resistant (left panel) and sensitive (right panel) cells.

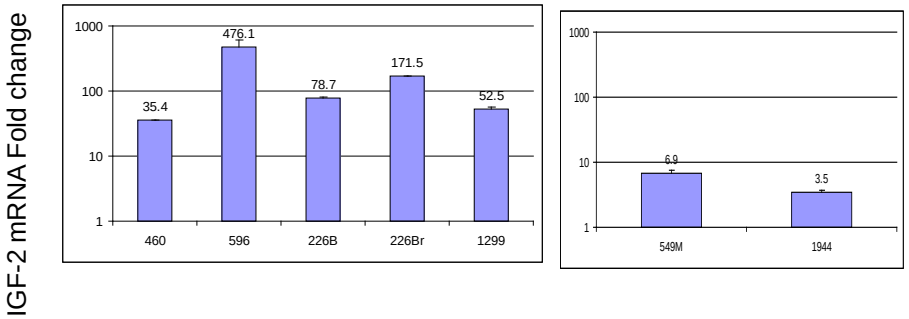

Figure 27. IGF-2 mRNA fold changes in the resistant and sensitive cells

RNA was isolated 48 h after 5uM of vorinostat treatment, and mRNA levels of IGF-2 and L32 were determined by quantitative real-time PCR. After the normalization by L32 control, mRNA expression levels between the untreated and vorinostat-treated samples in the resistant (left panel) and sensitive (right panel) cells.

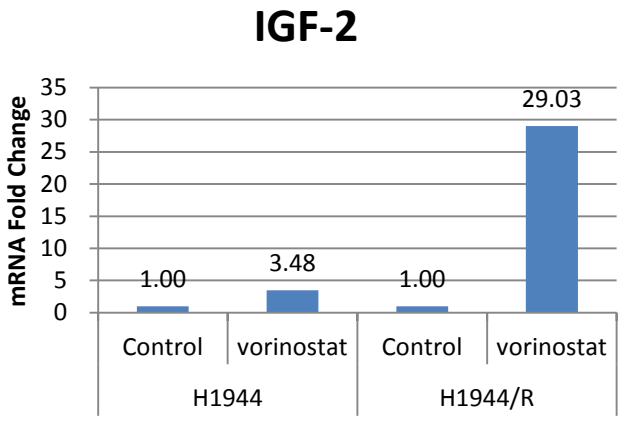

Figure 28. IGF-2 mRNA fold changes in H1944 and H1944R cells

RNA was isolated 48 h after 5uM of vorinostat treatment, and mRNA levels of IGF-2 and L32 were determined by quantitative real-time PCR. After the normalization by L32 control, mRNA expression levels between the untreated and vorinostat-treated samples in the H1944 (left panel) and H1944/R (right panel) cells.

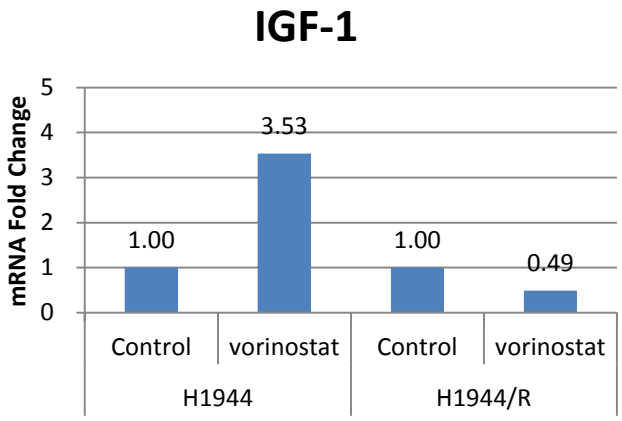

Figure 29. IGF-1 mRNA fold changes in H1944 and H1944R cells

RNA was isolated 48 h after 5uM of vorinostat treatment, and mRNA levels of IGF-1 and L32 were determined by quantitative real-time PCR. After the normalization by L32 control, mRNA expression levels between the untreated and vorinostat-treated samples in the H1944 (left panel) and H1944/R (right panel) cells.

IV. Discussion

In the present study, the activation of IGF-1R signaling might be *de novo* as well as acquired mechanism of resistance to vorinostat in NSCLC cells. NSCLC cells with persistent IGF-1R activity showed primary resistance to vorinostat. Chronic exposure to vorinostat is associated with enhanced IGF-1R activity in NSCLC cells resistant to vorinostat. Drug combinations with vorinostat and co-targeting IGF-1R may offer valid therapeutic approaches to overcome resistance to vorinostat.

Resistance to an anticancer treatment either present primarily in tumor cells or acquired during a treatment is a fairly common and persistent problem during cancer treatment. Acquired resistance is a particular problem, because tumors not only become resistant to the drugs originally used to treat them, but may also become cross-resistant to other drugs with different mechanisms of action (21). Although the precise mechanism of resistance to HDAC inhibitors has not been completely elucidated, cellular factors that have been implicated as determinants of resistance in HDAC inhibitors were discussed in a recent review (22): (a) drug efflux, (b) target overexpression and desensitization, (c) chromatin/epigenetic alterations, (d) stress response mechanisms, and (e) anti-apoptotic/prosurvival mechanisms. Also a nine-gene classifier has been suggested useful in predicting drug sensitivity, not resistance, to

HDAC inhibitors (19). More recently, constitutive activation of signal transducers and activators of transcription (STATs) were observed in vorinostat resistant CTCL cell lines, and immunohistochemical analysis of patient skin biopsy in phase IIb trial showed nuclear accumulation of STAT1 and high levels of nuclear phosphorylated STAT3 in malignant T cells correlate with a lack of clinical response (23). Consistent with these observation, co-treatment of another HDAC inhibitor, panobinostat, with JAK2/STAT tyrosine kinase inhibitor TG101209 exerted greater down-regulation of JAK2 and downstream STAT3 signaling, as well as greater cytotoxicity against primary CD34+ myeloproliferative neoplastic cells (24).

The activation of STAT3 protein by IGF-IR pathway was well established in vitro and in vivo (25-28), and our study confirmed that inhibition of IGF-1R pathway could overcome vorinostat resistance, which is known to be associated with STAT3 activity. IGF-1R has been implicated in resistance to various types of therapy in other cancer, including lung, breast, colorectal cancer, as well as hepatocellular carcinoma or melanoma (29-31). Furthermore, several published reports describing cell culture models of acquired resistance to both targeted agents and conventional chemotherapy drugs have similarly demonstrated the activation of IGF-1R in drug-resistant derivatives (32-34). More recently, the existence of drug-tolerant subpopulation that survive acute drug treatment through activation of IGF-1R signaling was demonstrated, and the drug-tolerant cells can be

selectively ablated by treatment with IGF-1R inhibitors (35). Noticeably, the authors also observed these drug-tolerant cancer cells were hypersensitive to HDAC inhibitors, which suggest a therapeutic opportunity to prevent the development of stable drug resistance.

It was observed that the increased phosphorylation of IGF-1R in the vorinostat resistant cells while the expression of IGF-1R was relatively stable. This observation provoked the need to investigate the changes of ligands, insulin-like growth factor 1 (IGF1) and IGF2. IGF2 binds to at least two different types of receptor: IGF-1R and mannose 6-phosphate/IGF2 receptor (M6-P/IGF-2R). Ligand binding to IGF 1R provokes mitogenic and anti-apoptotic effects. IGF2 appears to be involved in the progression of many tumors (36, 37). Dysregulation of genomic imprinting is one of the important factors that contribute to the increased expression of *IGF2* in tumor (38). In a case-control study, high plasma levels of IGF1 were associated with an increased risk of lung cancer while IGF2 was not associated with lung cancer risk (39). Contrastingly, circulating IGF1 concentrations did not seem to be related to lung cancer risk in a subsequent meta-analysis (40). In fact, IGF2 has been implicated to be a potent stimulator of tumor growth for NSCLC cells (41), and loss of imprinting of IGF2 was quite common event in lung cancer (42, 43).

In the present study, the increase of IGF-2 was identified in the vorinostat resistant NSCLC cells after exposure. Regulation of IGF-2 expression is very complicated in somatic cells. The hypomethylated

maternally inherited imprinting control region (ICR) binds the insulator protein CTCF and blocks activity of the proximal *Igf2* promoter by insulating it from its distal enhancers. Regulation of IGF2 expression involves a non-translated mRNA known as H19 and silencing of one allele by a genomic imprinting mechanism (44). A paternally methylated germ line differentially methylated region (DMR) between Igf2 and H19 is responsible for monoallelic expression of both H19 and Igf2 (45), and therefore, is called an imprinting control region (ICR). The regulatory functions of the ICR depend on allele-specific DNA methylation. The ICR immediately upstream of the H19 gene is essential for regulation of the entire locus and contains seven CTCF-binding sites in human (46). DNA methylation abrogates CCCTC-binding factor (CTCF) binding to these sequences and all sites demonstrate methylation-sensitive insulator activity (46, 47). On the maternal allele the ICR is unmethylated, CTCF is bound, and the Igf2 promoter is prevented from accessing the enhancers downstream of H19. The loss of CTCF binding results in an induction of maternal Igf2 similar to that caused by a deletion of the entire ICR, indicating a complete loss of enhancer blocking (48). Knock-down of CTCF by shRNA resulted in the loss of imprinting of IGF2 and the expression of maternal IGF2 was restored (49). Further studies are ongoing to reveal the exact mechanism of the IGF-2 activation in these vorinostat-sensitive and resistant cells.

One of the important observations in the present study is that the proliferation of NSCLC cells was not correlated with the level of inhibition of IGF-1R expression by monoclonal antibody in the monolayer culture condition (Fig 10 and 11). With the colony formation assays in soft agar, which is known to mimic 3D culture condition, the anti-proliferation effect of IGF-1R inhibition revealed in the resistant cells, and also was confirmed by xenograft experiments. Considering preclinical screening of investigational new drugs is a resource consuming process, we should also be prudent to discard the development if monolayer culture studies are misleading for the activity, especially for monoclonal antibodies. Further studies are warranted to investigate the mechanism which could lead these differential activities in monolayer and 3D culture conditions, but this would be beyond the scope of the current study.

V. Conclusion

Our results suggested that (a) resistance to vorinostat could be related to activation of IGF-1R through increased IGF-2 transcription and (b) integration of IGF-IR–targeted agents might overcome the resistance to vorinostat in patients with NSCLC. Results from this study provide a proof-of principle for clinical trials of dalotuzumab and vorinostat combination in patients with NSCLC.

VI. Reference

1. Jemal A, Siegel R, Ward E, Hao Y, Xu J, Thun MJ. Cancer statistics, 2009. CA Cancer J Clin. 2009;59(4):225-49.

2. Janku F, Stewart DJ, Kurzrock R. Targeted therapy in non-small-cell lung cancer--is it becoming a reality? Nat Rev Clin Oncol. 2010;7(7):401-14.

3. Sandler A, Gray R, Perry MC, Brahmer J, Schiller JH, Dowlati A, et al. Paclitaxel-carboplatin alone or with bevacizumab for non-small-cell lung cancer. N Engl J Med. 2006;355(24):2542-50.

4. Pirker R, Pereira JR, Szczesna A, von Pawel J, Krzakowski M, Ramlau R, et al. Cetuximab plus chemotherapy in patients with advanced non-small-cell lung cancer (FLEX): an open-label randomised phase III trial. Lancet. 2009;373(9674):1525-31.

5. Kwak EL, Bang YJ, Camidge DR, Shaw AT, Solomon B, Maki RG, et al. Anaplastic lymphoma kinase inhibition in non-small-cell lung cancer. N Engl J Med. 2010;363(18):1693-703.

6. Minucci S, Pelicci PG. Histone deacetylase inhibitors and the promise of epigenetic (and more) treatments for cancer. Nat Rev Cancer. 2006;6(1):38-51.

7. Richon VM, Garcia-Vargas J, Hardwick JS. Development of vorinostat: current applications and future perspectives for cancer therapy. Cancer Lett. 2009;280(2):201-10.

8. Ramalingam SS, Parise RA, Ramanathan RK, Lagattuta TF, Musguire LA, Stoller RG, et al. Phase I and pharmacokinetic study of vorinostat, a histone deacetylase inhibitor, in combination with carboplatin and paclitaxel for advanced solid malignancies. Clin Cancer Res. 2007;13(12):3605-10.

9. Kelly WK, O'Connor OA, Krug LM, Chiao JH, Heaney M, Curley T, et al. Phase I study of an oral histone deacetylase inhibitor, suberoylanilide hydroxamic acid, in patients with advanced cancer. J Clin Oncol. 2005;23(17):3923-31.

10. Marks PA, Breslow R. Dimethyl sulfoxide to vorinostat: development of this histone deacetylase inhibitor as an anticancer drug. Nat Biotechnol. 2007;25(1):84-90.

11. Mann BS, Johnson JR, He K, Sridhara R, Abraham S, Booth BP, et al. Vorinostat for treatment of cutaneous manifestations of advanced primary cutaneous T-cell lymphoma. Clin Cancer Res. 2007;13(8):2318-22.

12. Olsen EA, Kim YH, Kuzel TM, Pacheco TR, Foss FM, Parker S, et al. Phase IIb multicenter trial of vorinostat in patients with persistent, progressive, or treatment refractory cutaneous T-cell lymphoma. J Clin Oncol. 2007;25(21):3109-15.

13. Komatsu N, Kawamata N, Takeuchi S, Yin D, Chien W, Miller CW, et al. SAHA, a HDAC inhibitor, has profound anti-growth activity against non-small cell lung cancer cells. Oncol Rep. 2006;15(1):187-91.

14. Traynor AM, Dubey S, Eickhoff JC, Kolesar JM, Schell K, Huie MS, et al. Vorinostat (NSC# 701852) in patients with relapsed non-small cell lung cancer: a Wisconsin Oncology Network phase II study. J Thorac Oncol. 2009;4(4):522-6.

15. Owonikoko TK, Ramalingam SS, Kanterewicz B, Balius TE, Belani CP, Hershberger PA. Vorinostat increases carboplatin and paclitaxel activity in non-small-cell lung cancer cells. Int J Cancer. 2010;126(3):743-55.

16. Ramalingam SS, Maitland ML, Frankel P, Argiris AE, Koczywas M, Gitlitz B, et al. Carboplatin and Paclitaxel in combination with either vorinostat or placebo for first-line therapy of advanced non-small-cell lung cancer. J Clin Oncol. 2010;28(1):56-62.

17. Han JY, Oh SH, Morgillo F, Myers JN, Kim E, Hong WK, et al. Hypoxia-inducible factor 1alpha and antiangiogenic activity of farnesyltransferase inhibitor SCH66336 in human aerodigestive tract cancer. J Natl Cancer Inst. 2005;97(17):1272-86.

18. Lee HY, Moon H, Chun KH, Chang YS, Hassan K, Ji L, et al. Effects of insulin-like growth factor binding protein-3 and farnesyltransferase inhibitor SCH66336 on Akt expression and apoptosis in non-small-cell lung cancer cells. J Natl Cancer Inst. 2004;96(20):1536-48.

19. Miyanaga A, Gemma A, Noro R, Kataoka K, Matsuda K, Nara M, et al. Antitumor activity of histone deacetylase inhibitors in non-

small cell lung cancer cells: development of a molecular predictive model. Mol Cancer Ther. 2008;7(7):1923-30.

20. Gridelli C, Rossi A, Bareschino MA, Schettino C, Sacco PC, Maione P. The potential role of insulin-like growth factor receptor inhibitors in the treatment of advanced non-small cell lung cancer. Expert Opin Investig Drugs. 2010;19(5):631-9.

21. Dedes KJ, Dedes I, Imesch P, von Bueren AO, Fink D, Fedier A. Acquired vorinostat resistance shows partial cross-resistance to 'second-generation' HDAC inhibitors and correlates with loss of histone acetylation and apoptosis but not with altered HDAC and HAT activities. Anticancer Drugs. 2009;20(5):321-33.

22. Fantin VR, Richon VM. Mechanisms of resistance to histone deacetylase inhibitors and their therapeutic implications. Clin Cancer Res. 2007;13(24):7237-42.

23. Fantin VR, Loboda A, Paweletz CP, Hendrickson RC, Pierce JW, Roth JA, et al. Constitutive activation of signal transducers and activators of transcription predicts vorinostat resistance in cutaneous T-cell lymphoma. Cancer Res. 2008;68(10):3785-94.

24. Wang Y, Fiskus W, Chong DG, Buckley KM, Natarajan K, Rao R, et al. Cotreatment with panobinostat and JAK2 inhibitor TG101209 attenuates JAK2V617F levels and signaling and exerts synergistic cytotoxic effects against human myeloproliferative neoplastic cells. Blood. 2009;114(24):5024-33.

25. Moser C, Schachtschneider P, Lang SA, Gaumann A, Mori A, Zimmermann J, et al. Inhibition of insulin-like growth factor-I receptor (IGF-IR) using NVP-AEW541, a small molecule kinase inhibitor, reduces orthotopic pancreatic cancer growth and angiogenesis. Eur J Cancer. 2008;44(11):1577-86.

26. Zhang W, Zong CS, Hermanto U, Lopez-Bergami P, Ronai Z, Wang LH. RACK1 recruits STAT3 specifically to insulin and insulin-like growth factor 1 receptors for activation, which is important for regulating anchorage-independent growth. Mol Cell Biol. 2006;26(2):413-24.

27. Zong CS, Chan J, Levy DE, Horvath C, Sadowski HB, Wang LH. Mechanism of STAT3 activation by insulin-like growth factor I receptor. J Biol Chem. 2000;275(20):15099-105.

28. Ferlin M, Noraz N, Hertogh C, Brochier J, Taylor N, Klein B. Insulin-like growth factor induces the survival and proliferation of myeloma cells through an interleukin-6-independent transduction pathway. Br J Haematol. 2000;111(2):626-34.

29. Horndler C, Gallego R, Garcia-Albeniz X, Alonso-Espinaco V, Alonso V, Escudero P, et al. Co-expression of matrix metalloproteinase-7 (MMP-7) and phosphorylated insulin growth factor receptor I (pIGF-1R) correlates with poor prognosis in patients with wild-type KRAS treated with cetuximab or panitumumab: a GEMCAD study. Cancer Biol Ther. 2011;11(2):177-83.

30. Desbois-Mouthon C, Cacheux W, Blivet-Van Eggelpoel MJ, Barbu V, Fartoux L, Poupon R, et al. Impact of IGF-1R/EGFR cross-talks on hepatoma cell sensitivity to gefitinib. Int J Cancer. 2006;119(11):2557-66.

31. Villanueva J, Vultur A, Lee JT, Somasundaram R, Fukunaga-Kalabis M, Cipolla AK, et al. Acquired resistance to BRAF inhibitors mediated by a RAF kinase switch in melanoma can be overcome by cotargeting MEK and IGF-1R/PI3K. Cancer Cell. 2010;18(6):683-95.

32. Buck E, Eyzaguirre A, Rosenfeld-Franklin M, Thomson S, Mulvihill M, Barr S, et al. Feedback mechanisms promote cooperativity for small molecule inhibitors of epidermal and insulin-like growth factor receptors. Cancer Res. 2008;68(20):8322-32.

33. Dallas NA, Xia L, Fan F, Gray MJ, Gaur P, van Buren G, 2nd, et al. Chemoresistant colorectal cancer cells, the cancer stem cell phenotype, and increased sensitivity to insulin-like growth factor-I receptor inhibition. Cancer Res. 2009;69(5):1951-7.

34. Eckstein N, Servan K, Hildebrandt B, Politz A, von Jonquieres G, Wolf-Kummeth S, et al. Hyperactivation of the insulin-like growth factor receptor I signaling pathway is an essential event for cisplatin resistance of ovarian cancer cells. Cancer Res. 2009;69(7):2996-3003.

35. Sharma SV, Lee DY, Li B, Quinlan MP, Takahashi F, Maheswaran S, et al. A chromatin-mediated reversible drug-tolerant state in cancer cell subpopulations. Cell. 2010;141(1):69-80.

36. Pollak MN, Schernhammer ES, Hankinson SE. Insulin-like growth factors and neoplasia. Nat Rev Cancer. 2004;4(7):505-18.

37. Toretsky JA, Helman LJ. Involvement of IGF-II in human cancer. J Endocrinol. 1996;149(3):367-72.

38. Sakatani T, Kaneda A, Iacobuzio-Donahue CA, Carter MG, de Boom Witzel S, Okano H, et al. Loss of imprinting of Igf2 alters intestinal maturation and tumorigenesis in mice. Science. 2005;307(5717):1976-8.

39. Yu H, Spitz MR, Mistry J, Gu J, Hong WK, Wu X. Plasma levels of insulin-like growth factor-I and lung cancer risk: a case-control analysis. J Natl Cancer Inst. 1999;91(2):151-6.

40. Renehan AG, Zwahlen M, Minder C, O'Dwyer ST, Shalet SM, Egger M. Insulin-like growth factor (IGF)-I, IGF binding protein-3, and cancer risk: systematic review and meta-regression analysis. Lancet. 2004;363(9418):1346-53.

41. Zhu CQ, Popova SN, Brown ER, Barsyte-Lovejoy D, Navab R, Shih W, et al. Integrin alpha 11 regulates IGF2 expression in fibroblasts to enhance tumorigenicity of human non-small-cell lung cancer cells. Proc Natl Acad Sci U S A. 2007;104(28):11754-9.

42. Kohda M, Hoshiya H, Katoh M, Tanaka I, Masuda R, Takemura T, et al. Frequent loss of imprinting of IGF2 and MEST in lung adenocarcinoma. Mol Carcinog. 2001;31(4):184-91.

43. Suzuki H, Ueda R, Takahashi T, Takahashi T. Altered imprinting in lung cancer. Nat Genet. 1994;6(4):332-3.

44. Kaneda A, Feinberg AP. Loss of imprinting of IGF2: a common epigenetic modifier of intestinal tumor risk. Cancer Res. 2005;65(24):11236-40.

45. Phillips JE, Corces VG. CTCF: master weaver of the genome. Cell. 2009;137(7):1194-211.

46. Hark AT, Schoenherr CJ, Katz DJ, Ingram RS, Levorse JM, Tilghman SM. CTCF mediates methylation-sensitive enhancer-blocking activity at the H19/Igf2 locus. Nature. 2000;405(6785):486-9.

47. Bell AC, Felsenfeld G. Methylation of a CTCF-dependent boundary controls imprinted expression of the Igf2 gene. Nature. 2000;405(6785):482-5.

48. Schoenherr CJ, Levorse JM, Tilghman SM. CTCF maintains differential methylation at the Igf2/H19 locus. Nat Genet. 2003;33(1):66-9.

49. Ling JQ, Li T, Hu JF, Vu TH, Chen HL, Qiu XW, et al. CTCF mediates interchromosomal colocalization between Igf2/H19 and Wsb1/Nf1. Science. 2006;312(5771):269-72.

VII. 국문초록

비소세포폐암에서 히스톤탈아세틸화제에 대한 내성 기전

김진수

서울대학교 의과대학 의학과 (분자종양의학 전공)

서론: 히스톤 탈아세틸화 효소 (Histone deacetylase, HDAC)는 크로마틴의 구조를 조절하여 유전자의 발현을 조절하며 최근 혈액질환 또는 폐암을 포함한 고형암의 치료제로 개발되어 오고 있다. 그러나, 최근의 임상 연구 결과에 따르면 HDAC 억제제의 효과는 기대 이하였으며 그 내성을 일으키는 기전에 대해서는 잘 알려져 있지 않다. 본 연구에서는 비소세포 폐암에서 HDAC 억제제에 대한 내성 기전을 살펴보고자 한다.

방법: 14 개의 비소세포 폐암 세포주를 HDAC 억제제인 vorinostat 으로 처치한 뒤 MTT assay 를 이용하여 반응을 평가한다. 통상적인 세포 배양 방법으로는 생체내의 3 차원적인 성장 환경에서의 약제 효과를 정확히 평가할 수 없을 수 있으므로, 본 연구에서는 soft agar colony forming assay 를 이용하여 동시에 반응을 평가한다. 이상의 실험을 통해서 vorinostat 에 감수성과 내성을 보이는 세포주를 구분한 뒤, RTK profiling array kit 를

이용하여 내성 세포주에서 활성화되는 성장인자를 확인한 뒤 Western blot 을 이용하여 확인한다. 확인된 성장인자에 대한 억제제를 복합처치 하였을 때 세포 생존에 미치는 영향을 MTT assay 와 soft agar colony forming assay 를 이용하여 확인한다. 감수성을 보이는 세포주를 지속적으로 vorinostat 에 노출시켜 획득 내성을 유도하고, 두 세포주에서 위와 같은 방법으로 활성화된 성장인자를 확인하고, 그 억제제의 항 종양효과를 확인한다. 이후 nude mouse 에서 종양 이식 모델을 이용하여 vorinostat 의 내성기전을 극복할 수 있는지 생체 내에서 확인한다.

결과: MTT assay 를 이용하여 vorinostat 에 대한 IC_{50} 를 각각의 세포주에 대해서 확인하였다. Soft agar colony forming assay 로 얻은 결과와 이를 비교하여 14 개의 세포주 중 내성과 감수성을 보이는 대표적인 세포주를 구별하였다. 일차 내성을 가졌던 대표적인 세포주 들에서 용량, 시간 의존적으로 IGF-1R 과 IR 의 활성화가 일어나는 것을 확인하였다. 반면, 감수성을 보였던 세포주에서는 이러한 활성의 증가가 관찰되지 않았다. 항 IGF-1R 항체인 dalotuzumab 을 병합처치 하면 내성 세포주에서 세포 독성이 증가함을 확인하였다. 획득 내성을 가진 세포주에서 일차 내성을 보였던 세포주와 마찬가지로 IGF-1R 과 IR 의 활성화가 일어나는 것을 확인하고, dalotuzumab 의 복합처치로 세포 독성이 증가함을 확인하였다. 일차 또는 획득 내성을 보이는 세포주에서

vorinostat 처치로 인해 IGF-2 의 증가 유도되어 IGF-1R 의 활성화가 일어남을 확인하였다. 종양 이식 모델을 이용하여 vorinostat 에 대해서 일차 내성, 획득 내성을 보인 각각의 세포주에서 dalotuzumab 의 복합처치로 내성을 극복할 수 있음을 보였다.

결론: 이상의 결과를 통해서 HDAC 억제제인 vorinostat 에 대한 일차 또는 획득 내성의 기전이 IGF-1R 의 활성화와 관련되어 있을 가능성을 제시하였다. 또한, 항 IGF-1R 항체인 dalotuzumab 을 병합처치함으로서 이러한 내성을 극복할 수 있음을 제시하였다.

주요어: 비소세포폐암, 히스톤 탈아세틸화 효소 억제제, insulin-like growth factor, 약제 내성 기전

학번: 2005-30674